

Development of Frontal Boundaries During the Extratropical Transition of Tropical Cyclones

Evan Jones¹ | Rhys Parfitt¹ | Allison A. Wing¹

¹Department of Earth Ocean and Atmospheric Science, Florida State University, Tallahassee, Florida, 32311, United States of America

Correspondence

Evan Jones, Earth Ocean and Atmospheric Science, Florida State University, Tallahassee, Florida, 32311, United States of America
Email: ej18c@fsu.edu

Funding information

This study seeks to characterize the development of atmospheric fronts during the extratropical transition (ET) of tropical cyclones (TCs) as a function of their evolution during ET. Composite histograms indicate that the magnitude of the lower atmospheric frontogenesis and average sea surface temperature (SST) is different based on the nature of the TC's structural change during ET. We find that the development of cold and warm fronts evolves as expected from conceptual models of extratropical cyclones. Composites of these fronts relative to the completion of ET show that azimuth, storm motion, and deep-layer shear all appear to have equal influence on the frontal positions. TCs that have more fronts at the time of ET onset complete ET more quickly, suggesting that pre-existing fronts before ET begins may contribute to a shorter ET duration. The orientations of fronts at ET completion in the North Atlantic and West Pacific align with the climatological distributions of the SSTs associated with the western boundary currents in each of those basins. These results provide a perspective on the locations of frontal development within TCs undergoing ET.

KEYWORDS

extratropical transition, tropical cyclones, frontogenesis, western boundary current

1 | INTRODUCTION

As tropical cyclones (TCs) move poleward, they can undergo the process of extratropical transition (ET), where a TC loses its symmetric, deep-tropospheric warm core structure and becomes an extratropical cyclone (ETC). This occurs when the TCs encounter regions of higher baroclinicity, cooler sea surface temperatures (SSTs) and is accompanied by an expansion of their wind field and thermal asymmetry across the cyclone (Jones et al., 2003). The associated hazards with TCs undergoing ET often rival the hazards from TCs themselves, with a larger region of stronger winds and devastating storm surge. In particular, a hallmark sign of ET is the development of distinct cold and warm frontal boundaries as a result of interaction with a mid-latitude baroclinic zone (Sarro and Evans, 2022).

Individual case studies have demonstrated that the development of fronts during ET is dominated by the interaction between the TC's own circulation and a zonally-oriented baroclinic zone (Zhou et al., 2012), while a case study of Hurricane Matthew showed that the heaviest rainfall occurred where spiral rainbands intersected a near-surface front (Powell and Bell, 2019). More generally, Kitabatake (2008) analyzed a two-year time period in the Western North Pacific, showing that large-scale flows and sea surface temperature (SST) patterns are unique in that basin and may induce a unique ET process, where warm fronts develop near the center of the TC before completing their ET. Sarro and Evans (2022) demonstrated that for North Atlantic TCs, warm-seclusion cyclones have stronger frontogenesis in the lower-troposphere along their warm and bent-back fronts, and conversely stronger frontolysis in the lower-troposphere along their developed cold fronts. No study, to date, has fully characterized frontal development during the ET period globally.

Global climatologies of ET (Evans et al., 2017; Keller et al., 2019; Bieli et al., 2019a,b; Hart et al., 2006) and climate model simulations (Michaelis and Lackmann, 2019, 2021; Jung and Lackmann, 2021) show that of the roughly one-third of global TCs that undergo ET on an annual basis, a large majority of these do so within the vicinity of western boundary currents (WBCs), such as the Gulf Stream (GS) in the North Atlantic (NATL) and Kuroshio Extension in the Northwestern Pacific (WPAC). Indeed, previous work has shown that WBCs play an important role in the development of TCs and wintertime ETCs alike (Cione et al., 1993; Bright et al., 2002; Businger et al., 2005; Jacobs et al., 2008; Booth et al., 2012; Tsopouridis et al., 2020, 2021).

For ETCs, prior work has suggested that differences in surface forcing, particularly from SSTs, can lead to changes in the evolution of frontal development in ETCs. Using a case study of a mid-latitude winter cyclone near the GS, Jacobs et al. (2008) note that when the GS SST gradient (∇ SST) changed location, the locations of where fronts developed relative to the cyclone centers also changed. Booth et al. (2012) analyzed two different mid-latitude winter storms near the GS and modified both the absolute SST and strength of the ∇ SST, concluding that subsequent changes in a storm's intensity and structure can be attributed to latent heat flux in the storm's warm conveyor belt. They also suggest that the absolute SST is just as important as the ∇ SST strength for direct impacts on a storm's evolution. Other work has demonstrated that, more generally, SST gradients can drive significant sensible heat flux gradients, which in turn can produce regions of enhanced atmospheric frontogenesis (Parfitt et al., 2016; Reeder et al., 2021). In terms of TCs undergoing ET, Jones et al. (2023) found that there is a statistically significant difference in the strength of the ∇ SST associated with the unseparated GS in the days leading up to TCs either successfully or not successfully completing their ET in that region.

Indeed, while the case for large-scale atmospheric forcing driving ET is well-established, such as favorable phasing with an upper-level trough or jet stream (Jones et al., 2003; Hart et al., 2006), the question of whether or not ET is, to first order, dominated by large-scale forcing in the upper-atmosphere, or if it can be forced by surface-based processes is still an open question. Of particular relevance here are the studies by Hart et al. (2006) and Sekioka (1957) speculating that, in the absence of strong large-scale atmospheric forcing, baroclinicity induced from surface

forcing could perhaps lead to ET.

Given the aforementioned work detailing the development of fronts in midlatitude winter cyclones and the growing evidence in high-resolution data for surface-based forcing of frontal development, this motivates a characterization of the development of fronts in TCs that undergo ET. As such, the purpose of this study is to characterize the evolution of frontal development as ET progresses, both from a global perspective and also in specific ocean basins. Section 2 presents the data and methods used for this work. Section 3 presents the results. Section 4 summarizes the findings, describes limitations of these results, and motivates areas for future work.

2 | DATA AND METHODS

2.1 | Data

2.1.1 | ERA5 Reanalysis

This work uses the European Center for Medium-Range Weather Forecasts (ECMWF) ERA5 reanalysis dataset, which employs a model resolution of TL639 while the output is available at a horizontal resolution of $0.25^\circ \times 0.25^\circ$ (Hersbach et al., 2020). From ERA5, the variables we use are geopotential height, temperature, u- and v-winds and sea surface temperature. While ERA5 does not feature any vortex relocation or insertion of TC wind profile retrievals, as other reanalyses do (such as CFSR, see Saha et al. 2010; MERRA-2, see McCarty et al. 2016; JRA-55, see Kobayashi et al. 2015; and NOAA-20C, see Compo et al. 2011), it is currently one of the highest resolution reanalyses available. Prior work has shown that reanalyses systematically underestimate TC intensity in terms of both MSLP and 10-m maximum wind speed relative to the best track in all basins Schenkel and Hart (2012), while newer reanalyses with improved bias correction schemes and corrections in TC position and structure tend to reproduce TCs better (Hodges et al., 2017). TCs in global climate models are sensitive to convective parameterizations (Duvel et al., 2017; Kim et al., 2012; Murakami et al., 2012; Reed and Jablonowski, 2011; Zhao et al., 2012), while other work has shown that there is no significant improvement in TC activity in a reanalysis compared to its corresponding free-running model simulation (Aarons et al., 2021). Nevertheless, ERA5 has been shown to have improvements over other reanalyses in TC representation in terms of the environment surrounding TCs (Slocum et al., 2022), inner core representation and TC precipitation (Jones et al., 2021). Although biases are known to exist in ERA5 as noted above, they are generally small enough to support usage of ERA5 for higher-resolution studies (Seethala et al., 2021). Thus, ERA5 can capture frontal development on the order of 100-km scale, which past work has indicated as a sufficient scale for analyzing these interactions (Parfitt et al., 2016, 2017).

2.1.2 | TempestExtremes

We examine the set of TC tracks in ERA5 from Zarzycki et al. (2021), which were derived in that study by applying TempestExtremes (Ullrich and Zarzycki, 2017; Zarzycki et al., 2017; Zarzycki and Ullrich, 2017) over the period from 1980-2018. TempestExtremes detects TCs in each reanalysis by first identifying a minimum in SLP surrounded by a closed contour of pressure. Then a 300-500hPa geopotential thickness maximum must be located horizontally within 1° of the identified TC center to track only warm-core cyclones. TC position, intensity and maximum 10-meter winds are provided every six hours. As TCs tracked using TempestExtremes are primarily used to capture TCs as tropical systems, a cyclone may not be tracked through its entire lifecycle, including after it starts and completes ET, although we expect the majority of TCs that complete ET to be captured in ERA5. We do not extend tracks into the extratropical

phase, since the analysis is primarily focused on the actual process of ET itself. Prior studies of ET (e.g., Bieli et al., 2019a) also used tracks that were not extended into the extratropical phase. ERA5 has slightly high biases in TC days compared to the best-track; Zarzycki et al. (2021) note this could be due to tracks extending well past the ET process, even though this is not the intent of the TempestExtremes tracking algorithm for TCs (possible reasons for this are discussed in Section 3.1). Using TempestExtremes, ERA5 has some of the highest hit rates for TC counts compared to other reanalyses, though a somewhat higher false alarm rate (Zarzycki et al., 2021). To ensure the validity of our results and the lack of a need to extend trajectories into the extratropical phase given our focus only on the ET process itself, we conducted some sensitivity analysis to determine the effects of the tracker on the CPS results. Our conclusions are qualitatively similar whether we use any of the following three trajectory datasets: the TempestExtremes tracks from ERA5 from Zarzycki et al. (2021), the tracks from Jones et al. (2021) that were based on IBTrACS (Knapp et al., 2010), or IBTrACS trajectories extended using ExTraTrack (Zarzycki et al., 2017) to include the extratropical phase from Bower et al. (2022) (not shown).

2.2 | Methods

2.2.1 | Cyclone Phase Space

To analyze the life cycle of TCs as they undergo ET, we use the cyclone phase space (CPS) framework created by Hart (2003). While other identifiers for ET have been noted in the literature, such as using potential vorticity inversion (Zhou et al., 2012; Li and Wang, 2013; Kofron et al., 2010), the CPS is routinely used in operational forecasting and research. The life cycle of atmospheric cyclones is quantified in the CPS based on a cyclone's thermal structure and thickness asymmetry within a 500-km great circle distance from its center (following the methods of Hart 2003, which introduced the CPS, as well as other studies analyzing CPS metrics). Since the orientation and location of fronts relative to the cyclone center can vary and be somewhat unpredictable, the 500-km symmetric radius ensures we capture fronts wherever they occur. Three parameters are used to diagnose position within the CPS: thickness asymmetry across the cyclone (B), lower tropospheric thermal wind ($-V_T^L$) and upper tropospheric thermal wind ($-V_T^U$). The B parameter diagnoses the asymmetry across the cyclone and identifies the strength of the non-frontal ($B < 10$) or frontal ($B > 10$) nature of the cyclone according to the following equation:

$$B = h(\overline{Z_{600hPa} - Z_{900hPa}}|R - \overline{Z_{600hPa} - Z_{900hPa}}|L), \quad (1)$$

where Z is the geopotential height at a specified pressure level, R refers to right of the storm motion vector, L refers to left of storm motion vector, and h is a scaling parameter based on hemisphere ($h=1$ for the Northern Hemisphere and -1 for the Southern Hemisphere).

The parameters $-V_T^L$ and $-V_T^U$ are defined as the following:

$$-V_T^L = \frac{\delta \Delta Z}{\delta(\ln \rho)} \bigg|_{900hPa}^{600hPa} \quad (2)$$

$$-V_T^U = \frac{\delta \Delta Z}{\delta(\ln \rho)} \bigg|_{900hPa}^{300hPa}, \quad (3)$$

where Z is the geopotential height at pressure levels between the specified bounds and a linear regression is fit over seven regular pressure levels in 50hPa increments across those bounds, inclusive. Positive values of $-V_T^L$ and $-V_T^U$ indicate a warm core cyclone (TC if both values are positive, and subtropical or warm-seclusion ETC if $-V_T^L$ is positive and $-V_T^U$ is negative), while negative values of both indicate a cold core ETC. While CPS parameters are typically calculated as a 24-hour running mean, we use the instantaneous 6-hourly values of each parameter to better match with frontal development at simultaneous times, and also use these parameters as dimensionless and normalized by their units, similar to previous work (Bieli et al., 2019a). While using the smoothed values produces some slight quantitative differences, the trajectories of cyclones within the CPS based on the instantaneous and smoothed CPS parameters are qualitatively similar (not shown).

An example CPS diagram is shown in Figure 1. For contextualizing different phases of ET using the CPS, we define “ET onset” as the time within a TC’s trajectory when its lower tropospheric thermal wind is greater than zero and its thickness asymmetry is greater than 11, i.e., when it enters the top right quadrant of Figure 1. “ET completion” is defined as the first time within the lifecycle of a TC when its lower tropospheric thermal wind is less than 0 and its thickness asymmetry is greater than 11 (when it enters and terminates in the top left quadrant of Figure 1). Both of these definitions are similar to that used by Bieli et al. 2019a, who also used the CPS to identify ET in reanalyses. There are some TCs that transition through the lower-left quadrant of the CPS, though we focus on the idealized path through the CPS (red arrow) that most transitioning TCs take globally and in the NATL, as noted by Evans et al. 2017 and Bieli et al. 2019a. This is in order to have a sufficient number of samples for taking composites and to limit variability in ET path, though a comparison of the presented results to CPS paths through the lower-left quadrant of the CPS warrants further work. Bieli et al. 2019b note that the CPS-based classification of ET agrees best with the best-track classification in reanalyses in the WPAC in two other reanalyses (where roughly 80% of TCs are correctly identified compared to the best-track classifications) and NATL (where roughly 77% of TCs are correctly identified compared to the best-track observations). Jung and Lackmann (2021) note that there are issues with the detection of ET completion in high resolution datasets, where some storms retain a strong remnant warm core.

2.2.2 | Objective Frontal Identification

Currently, there is no consensus regarding an official definition of a front. Many previous studies have applied various methods of identifying fronts, with varying degrees of sensitivities to the method based on the application (Schemm et al., 2018; Spensberger and Sprenger, 2018; Thomas and Schultz, 2019). One way that fronts have been identified in prior work is by using objective diagnostics: a thermal parameter (Hewson, 1998) or a combination of both thermal and dynamical parameters (Parfitt et al., 2017) are selected to identify local gradients in vorticity and temperature advection. Diagnostics such as these have been used in previous work to analyze climatological frontal frequencies (Parfitt et al., 2016), global precipitation patterns across reanalysis datasets (Soster and Parfitt, 2022) and climate modes (Lawrence et al., 2022).

To capture characteristics of both temperature and vorticity when identifying frontal development during ET, we use the F diagnostic (Parfitt et al., 2017). The F diagnostic is based on the following equation:

$$F = \frac{\zeta_p |\nabla T_p|}{f |\nabla T_o|}, \quad (4)$$

where T is the temperature and ζ is the relative vorticity at a particular pressure level p , f is the Coriolis parameter and T_o is a typical temperature gradient defined as $0.45 \text{ K } (100 \text{ km})^{-1}$. To analyze the lower level atmospheric frontal

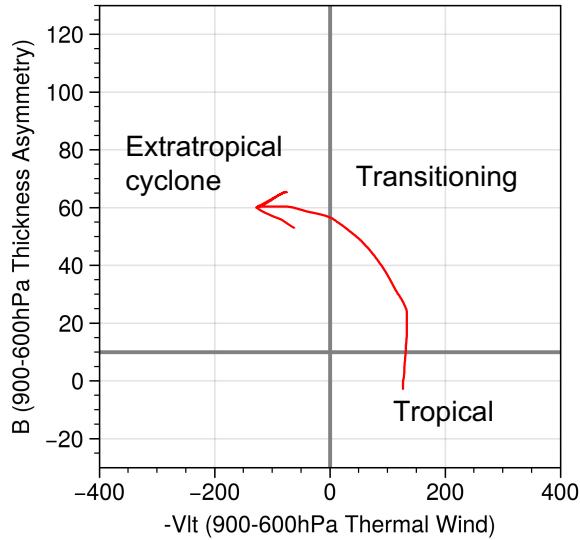


FIGURE 1 Cyclone phase space (CPS) framework from Hart (2003) based on the 900-600hPa thickness asymmetry (B parameter on the y-axis) and 900-600hPa thermal wind ($-V_T^z$ parameter on the x-axis) Labels inside indicate the general storm structure during its transition, and the red arrow is an idealized trajectory of a TC undergoing ET through the CPS.

development, the F diagnostic is calculated at the 900 hPa level. The F diagnostic must exceed a value of 1 to be identified as a front. Fronts are further partitioned as cold or warm fronts based on thermal advection (TA) at each identified front, as in Soster and Parfitt 2022, according to the following equation:

$$TA = -v_\rho \frac{\nabla(T_\rho)}{|\nabla T_\rho|}, \quad (5)$$

where v is the wind and T is the temperature at 900hPa. A cold front is identified when TA is less than -1.5 m s^{-1} , while warm fronts are identified when TA is greater than 1.5 m s^{-1} . When analyzing storm-centered composites of the F diagnostic, we mask locations where temperature gradients at 900 hPa are less than 0.02 K km^{-1} in order to remove possible spurious frontal identification by the F diagnostic as a result of intense vorticity near the TC center. We also use an additional criteria that in order for a grid point to be classified as frontal, it must also be contiguously connected to other grid points spanning 500 km. We utilize the F diagnostic calculations from Soster and Parfitt (2022). As in Soster and Parfitt (2022), we use a 500-km length criteria to avoid misclassifying local regions of high relative vorticity or temperature gradients not associated with fronts (for example, as can often occur at coastlines) as atmospheric fronts. Previous work has also used similar synoptic-scale length criteria (e.g. Schemm and Sprenger, 2015; Schemm et al. 2015).

2.3 | Frontogenesis

As an additional measure of frontal development, we consider the frontogenesis function, which includes both adiabatic and diabatic components (Petterssen, 1936). Numerous past studies have indicated that fronts are influenced by many processes including deformation, producing strong gradients in velocity and temperature (Bluestein, 1993), as well as from changes in the potential temperature gradient from various sources of heating, including sensible or latent heat flux (as noted by Reeder et al. 2021). Many studies also use frontogenesis as a proxy for frontal development in climate models and reanalyses, though there is sensitivity to resolution (Jenkner et al., 2010) and model physics (Mak et al., 2017). The frontogenesis equation (FGEN) is defined according to the following equation:

$$\text{FGEN} = 0.5|\nabla\theta|[D \cos(2\beta) - \delta] + \frac{\nabla\theta}{|\nabla\theta|} \cdot \nabla\hat{\theta}, \quad (6)$$

where θ is the potential temperature, D is the total deformation, β is the angle between isentropes and axis of dilatation, and δ is the divergence, all at a particular pressure level. $\nabla\theta$ is the ∇ of potential temperature and $\hat{\theta}$ is the diabatic heating rate (calculated in ERA5 as the full material derivative), with the gradient defined as normal to the isentropes pointing towards higher values.

3 | RESULTS AND DISCUSSION

3.1 | CPS Analysis Composites

To illustrate the spatial distribution of TCs undergoing ET within the CPS, we calculate a composite histogram of CPS position for all TCs that undergo ET globally (Figure 2, left panel). There are a total of 790 TCs that undergo ET that enter into the composites, representing roughly 25% of the total number of TCs in the TempestExtremes dataset. This is slightly lower than the average number globally given in climatologies in the literature (Bieli et al. 2019a state that roughly 33% of TCs undergo ET in the global average), but is a reasonable number given that TempestExtremes' purpose is to track tropical systems. ERA5 may also miss some TCs that occurred in nature, a common bias of reanalyses (Jones et al., 2021; Zarzycki et al., 2021). Globally, more TCs undergo ET through the upper right quadrant before becoming extratropical, as opposed to transitioning through the lower left quadrant prior to becoming extratropical. The middle and right panels of Figure 2 show the distribution of 900hPa frontogenesis and SST, defined here as the average within a 500-km radius from the TC center and composited based on CPS position. Globally, the composite shows that during ET, fronts preferentially form for storms that first become asymmetric and maintain their warm core structure (upper right quadrant), while SSTs are colder on average for storms that lose their warm core structure prior to becoming asymmetric (upper left quadrant). Similar behavior is seen when we separately consider Northern Hemisphere and Southern Hemisphere storms. The greatest frontogenesis is found during the most common pathway of ET (upper right quadrant) while coldest SSTs are found for storms that have reached the extratropical phase (upper left quadrant). It is possible that the number of storms in the extratropical phase (upper left quadrant), and thus the frontogenesis, is underestimated since we do not extend the TempestExtremes tracks further. Some TempestExtremes tracks extend well beyond the ET phase; this could be due to shear and warm seclusions, which the CPS has difficulty representing. Storms in highly sheared flow or without precipitation near the storm center will be tracked less effectively than those in low-shear environments that maintain latent heating near the storm center (C. Zarzycki, personal communication). Some TCs, such as Hurricane Sandy, maintain a deep warm core despite undergoing ET

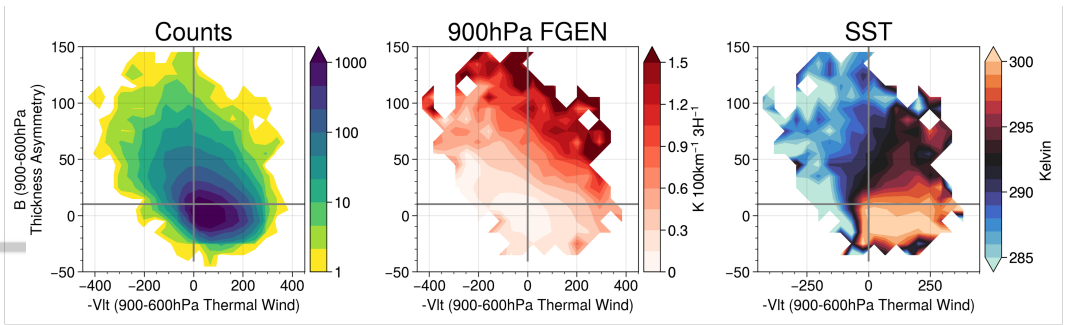


FIGURE 2 Composites of global TCs that have successfully completed ET, showing the (a) number of storm track points, (b) 900hPa frontogenesis and (c) SST with respect to the CPS. The latter two panels are defined as the average within a 500-km radius from the TC center at each timestep and average for that binned location within the CPS (Bin widths of 45 on the x-axes and 10 on the y-axes).

(Galarneau et al., 2013) and would thus be tracked longer by TempestExtremes (which tracks systems based on a mid-upper tropospheric thickness maximum) compared to TCs that develop shallow warm seclusions (see Sarro and Evans (2022) for more details). Overall, these results are consistent with our expectation that storms undergo ET as they move poleward into regions of colder SST and higher baroclinicity, and ultimately develop fronts.

3.2 | General Frontal Development During ET

Next, we analyze the frontal development at different vertical levels by calculating frontogenesis at 6 hourly increments within a 500 km radius from the TC center at 300 hPa, 600 hPa, and 900 hPa. Anomalies are calculated at each time step relative to the time of ET onset, as well as relative to the time of ET completion, for all storms that undergo ET through the upper right quadrant of the CPS. We consider the western North Pacific (WPAC; 405 storms) and North Atlantic (NATL; 174 storms) separately, as shown in Figure 3. For reference, the average frontogenesis values at the zero hour for both ET onset and ET completion at the three levels and in each basin are shown in Table S1 in the Supporting Information. The anomalies shown in Figure 3 are all frontogenetic relative to a lag of zero for both ET onset and ET completion.

Leading up to ET onset, TCs in both the WPAC and NATL show an increase in the average frontogenesis at all three pressure levels, though there is a faster increase in frontogenesis at lower levels. Units on the changes to frontogenesis anomalies are $\text{K } 100 \text{ km}^{-1} \text{ 3H}^{-1} \text{ 6H}^{-1}$. In the WPAC, the largest rates of increase in frontogenesis anomalies relative to ET onset at each level is 0.0039 at 300 hPa, 0.0099 at 600 hPa, and 0.014 at 900 hPa. In the NATL, the largest rates of increase in frontogenesis anomalies relative to ET onset at each level is 0.0085 at 300 hPa, 0.0095 at 600 hPa, and 0.014 at 900 hPa. After ET onset, the rates of increase in anomalies of frontogenesis generally level out, though they do so at each level with different timing relative to ET onset. The rate of increase slows and becomes approximately constant after ET onset first at 300 hPa, then at 600 hPa and finally levels out at 900 hPa approximately 18 hours after ET onset.

With respect to ET completion, the average frontogenesis slightly decreases leading up to the ET completion time at 300 hPa for TCs in both basins, while it increases and peaks just before or at the time of ET completion at 600 hPa and 900 hPa. In the WPAC, the largest rates of increase in frontogenesis anomalies relative to ET completion is

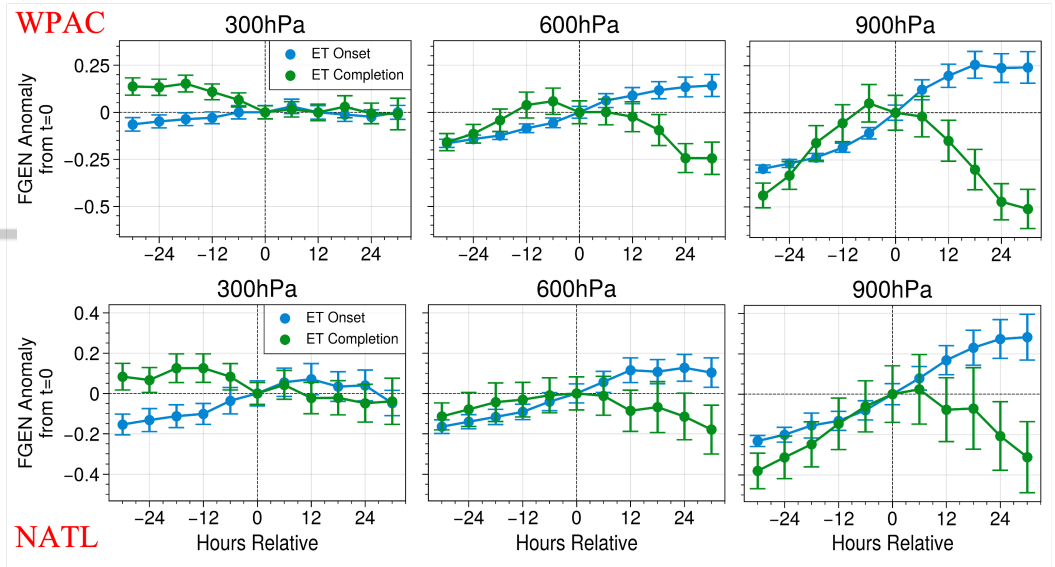


FIGURE 3 Anomalies of frontogenesis (units $\text{K } 100 \text{ km}^{-1} \text{ 3H}^{-1}$) averaged within 500 km of the storm center at different tropospheric levels relative to the time of ET onset (blue) and ET completion (green) in the WPAC (top) and NATL (bottom). Error bars indicate the 95% confidence interval in each 6-hourly increment.

0.0013 at 300 hPa, 0.013 at 600 hPa, and 0.023 at 900 hPa. In the NATL, the largest rates of increase in frontogenesis anomalies relative to ET onset is 0.0049 at 300 hPa, 0.0059 at 600 hPa, and 0.016 at 900 hPa. The decreases in average frontogenesis anomalies after ET completion are larger in a similar manner at lower levels compared to upper levels.

The reasons for this difference in the timing of the peak frontogenesis between basins are unclear, though asymmetries between the evolution of ET between basins may play a role, as well as differences in spatial distributions of phasing with upper-level atmospheric features during the ET process within each basin. Overall, the rate of increase of frontogenesis in the time leading up to ET completion is greatest at 900 hPa. The confidence intervals for NATL TCs are generally larger than for WPAC TCs. It is important to note that some TCs have ET durations longer than 30 hours (as noted by Bieli et al. 2019a), which means that there is likely some overlap between samples in some of the hour bins in Figure 3 at a given lead or lag relative to the time of ET onset or ET completion. Overall, this analysis indicates that the dominant frontogenetical responses occur in the lower troposphere, with larger changes in frontogenesis relative to ET onset and ET completion occurring at 900hPa. The rest of the results will thus focus on frontal development near the surface.

Storm-centered composites of cold and warm frontal frequencies using the F diagnostic at 900hPa show the evolution and structure of atmospheric fronts relative to the time of ET onset and ET completion (Figure 4). The colorbar extents are lower for the cold fronts than the warm fronts in Figure 4 and subsequent storm-relative composites of the F diagnostic in order to visualize the spatial variability of cold fronts despite their lower frequency. The development of cold and warm fronts is primarily due to advection of cold and warm air around an atmospheric disturbance. In marine ETCs specifically, the expected positions of developing cold and warm fronts is predominantly based on

the Shapiro and Keyser model (1990), where a warm front extends on the northern and eastern side of the cyclone center, while a cold front initially extends south and westward of the center, and wraps back around. The cold and warm fronts are delineated using the TA parameter described in Section 2.2.2. Frontal frequencies at any given point in Figure 4 and subsequent figures are calculated based on the total number of either cold or warm fronts that are identified at that given point divided by the total number of TC snapshots that fall into each bin. The results are shown in polar coordinates in order to identify the frontal positions as a function of distance from the TC center and angle relative to poleward. Poleward is oriented at 0° bearing.

As ET onset occurs (left panels in Figure 4), the warm fronts form at around 45° relative to poleward (i.e., to the northeast of the TC center in the Northern Hemisphere), before approaching closer to 90° (east of the TC center in the Northern Hemisphere) 24 hours after ET onset. The cold fronts have a much less banded structure than the warm fronts, but generally form between a 180° and 270° from poleward. We speculate that there are higher frequencies of warm fronts in the direction of storm motion ahead of the storm and higher frequencies of cold fronts opposite the direction of storm motion behind the storm due to warm air advection ahead and cold air advection behind the systems. There is also evidence for pre-existing cold fronts located poleward and left of the TC centers as ET onset approaches, where there are larger values of cold frontal frequency (at -12h and 0h in Figure 4). As these higher cold frontal frequency values occur far from the center, we speculate that these are most likely fronts not associated with the TC starting to undergo ET, but rather are evidence of the TC encountering a more favorable baroclinic environment for their ET to begin. Jung and Lackmann (2021) note that the baroclinic energy conversion increases while the surface latent heat flux decreases through the ET process for the storms they model. Their storm is both maintained and strengthened by surface diabatic heat fluxes in general until ET completion, with any post-ET reintensification a result of baroclinic energy conversion (see also Hsieh and Cook 2008). They also see that the maxima of kinetic energy in both of their control and future climate simulations are created at least somewhat by the conversion from eddy available potential energy via baroclinic conversion in the poleward region of the transitioning storm associated with warm air rising over the frontogenesis region. Thus, the locations of the maxima in diabatic heating and surface latent heat fluxes and the spatial scales of the baroclinic zones are crucial for how ET evolves. This would tie directly to where and how the fronts develop as we show, as the frontal formation has been established to be influenced by where surface conditions are more favorable for their development, such as near SST fronts.

Near the time of ET completion (right panels in Figure 4), the highest frequency of warm fronts is within the 45° to 90° range, though the frequency distributions become noisier after ET completion, likely due to a decreasing sample size from the TempestExtremes tracks as well as fronts perhaps starting to decay once ET completes. The spatial distribution of cold fronts continues to not have as pronounced of a banded structure, though the highest frequency of cold fronts is found between approximately 180° and 300°. After ET completion, the frequency of cold fronts decreases. While there is overall a higher frequency and coherent structure of warm fronts, they generally occur less frequently in overall frontal climatologies outside of the ET process (see Soster and Parfitt (2022) as an example). Since we are analyzing the specific process of frontal development during the ET of TCs, there are more warm fronts here simply because TCs are always bringing warmer, tropical air into the region. These global composites of the development and spatial distribution of warm and cold fronts during ET generally matches the conceptual models mentioned above of frontal locations as the literature suggests, with warm fronts extending poleward and eastward of the center, and cold fronts south and west of the center (Klein et al., 2000; Evans et al., 2017). While there is some slight quantitative sensitivity of the frontal diagnostic used for identifying fronts (see Figure S1 in the supplementary information comparing the F diagnostic with another frontal diagnostic from Hewson 1998), the choice of diagnostic does not qualitatively impact the overall results we present. Separating the analysis in Figure 4 between the NATL and WPAC shows qualitatively similar results, though the NATL composites appear noisier (not shown).

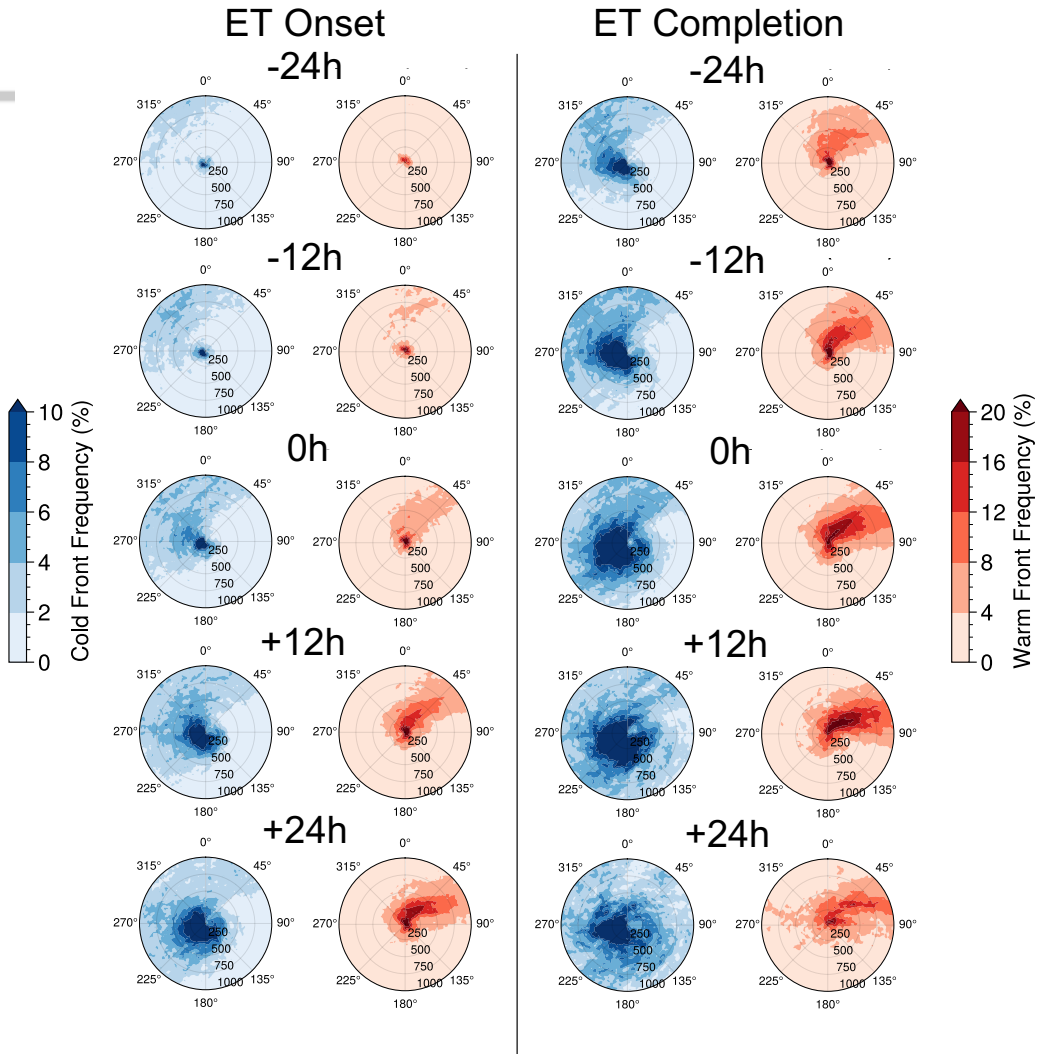


FIGURE 4 Storm-centered composites of cold (blue shading) and warm (red shading) frontal frequencies for global TCs as a function of time relative to ET onset (left) and ET completion (right). Plots are converted to polar coordinates based on distance in km from the center and degrees, with poleward oriented at 0° .

3.3 | Comparison of Frontal Development and Orientation

The analysis in the previous section considers the spatial distribution of fronts relative to poleward. However, the storm-centered composites may also be re-oriented relative to other directions to identify possible controlling factors of frontal orientation. Frontal frequency composites are calculated based on rotating the polar coordinates to align with the storm motion vector at each time step (calculated as the centered difference between the TC's position at consecutive 6-hourly timesteps and converted to a bearing) and the 300-850hPa environmental wind shear (defined as the vector difference of the mean wind magnitude and direction at 850hPa subtracted from the mean wind magnitude and direction at 300hPa, masking out the 500-km radius closest to the TC center to avoid contamination of the shear by the high winds of the TC itself; see Velden and Sears 2014, as an example using similar methodology).

Storm-centered composites of the cold and warm fronts at the time of ET completion for each orientation of the polar coordinates are shown in Figure 5. Warm fronts preferentially occur poleward and right of center, in the direction of storm motion, and predominantly left of the shear vector (and downshear), though there are some smaller values of warm frontal frequency to the right of the shear vector. The distribution of warm fronts covers a slightly wider range of azimuths in the poleward-relative and shear-relative composites compared to the storm motion-relative composites, but the spatial distribution and magnitude of the warm frontal frequencies is qualitatively similar across each composite, just rotated in different directions. This is also true for the cold fronts, as seen in the bottom of Figure 5. Cold fronts preferentially occur left of poleward, opposite the storm motion, and also opposite the shear vector (upshear). The lack of banded structure and wide range of azimuths over which cold fronts are found is seen in each composite. These results indicate that azimuth, storm motion, and deep-layer shear all appear to have equal influence on the frontal positions, since the distributions are somewhat similar.

At ET completion, most TCs are moving generally poleward and are recurving into the westerlies (Bieli et al., 2019a). Since the storm motion is primarily determined by the large-scale flow (Emanuel, 2018), at ET completion the storm motion would typically have a component that is from west to east. The mean storm motion vector magnitude is 18.1 m s^{-1} and the mean direction is 85.2° (from west to east), while the mean 300-850 hPa shear vector magnitude is 12.4 m s^{-1} and the mean direction is 93.3° (from west to east). The occurrence of warm fronts poleward and right of center is thus consistent with their position in the direction of storm motion and also in the same general direction as the shear vector. This makes sense because the shear is also determined by the large-scale flow that the TC is embedded in. The distribution of fronts at ET completion relative to both the storm motion and shear vectors is consistent with the poleward-relative distribution, given the typical large-scale flows that TCs undergoing ET encounter. We speculate that the patterns near the centers of the composite panels in Figure 5 is likely an artifact of conversion from latitude-longitude coordinates into polar coordinates, as well as errors in storm structural representation arising from the use of a 0.25° horizontal output resolution reanalysis. In addition, while our tracked storm centers are on model grid points, the "true" storm center may lie between grid points.

3.4 | ET Duration

The amount of time a TC takes to go from ET onset to ET completion (called ET duration in this section) could be related to how and when the fronts develop during ET. The PDF of ET duration for global TCs undergoing ET is shown in the left panel of Figure 6, with a sharp peak at 18 hours and an average time of approximately 36 hours. This average ET duration value is consistent with prior work; Bieli et al. (2019a) note that in their analysis, the average ET duration is 1-2.5 days, while Evans and Hart (2003) find an average ET duration of 33 hours for the NATL.

The relationship between ET duration and mean frontal frequencies at ET onset is further explored in the right

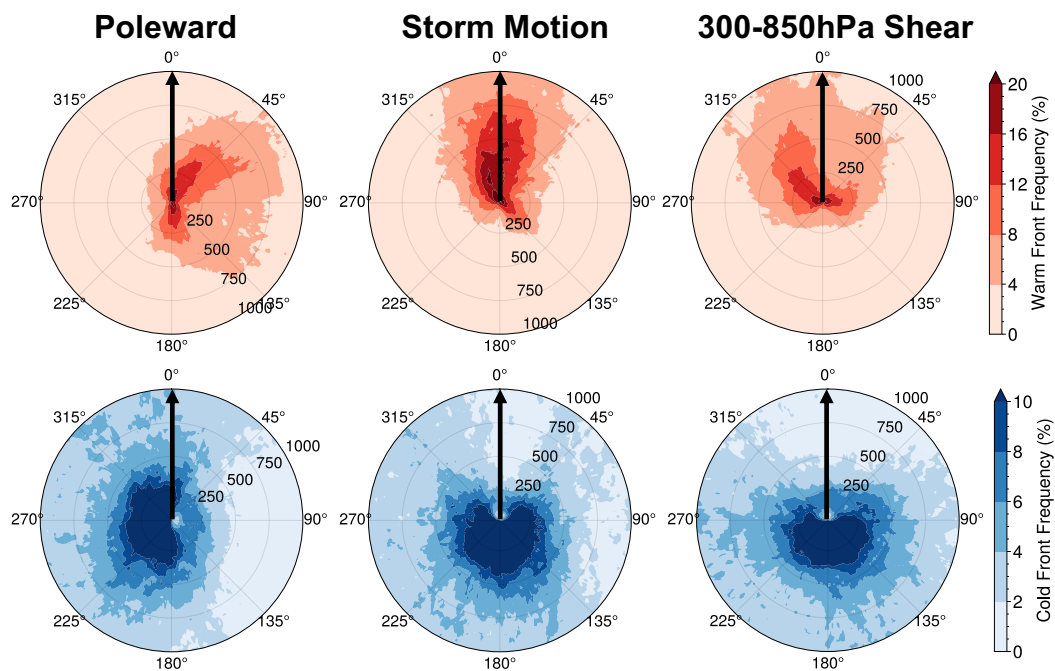


FIGURE 5 Storm-centered composites of the frontal frequencies for global TCs at ET completion for warm fronts (top) and cold fronts (bottom) with 0° azimuth defined as poleward (left), in the direction of the the storm motion vector (middle) in the direction of the 300-850mb environmental shear (right).

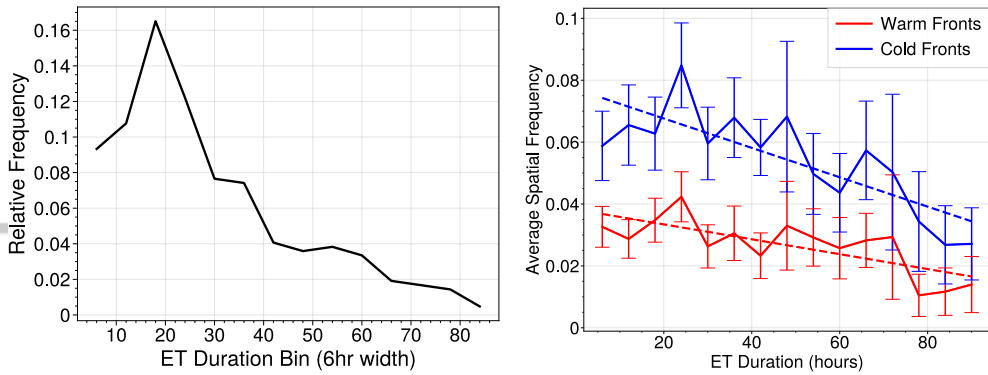


FIGURE 6 (Left) PDF of ET duration for global TCs that undergo ET as defined within the CPS in 6-hourly bins. (Right) Average spatial frequency of frontal points for warm fronts (red; taken between bearings of 0° to 45°) and cold fronts (blue; taken 225° to 315° for cold fronts) at ET onset as a function of ET duration in similar 6-hourly bins. Dashed lines indicate the line of best fit for each frontal type across the ET duration bins, and error bars show the 90% confidence intervals for the mean in each bin.

panel of Figure 6. The means are taken according to the regions in which the highest frequencies occur in the composites in Figure 4 (0° to 45° for warm fronts, 225° to 315° for cold fronts). The percentage of fronts outside of the specified quadrants for warm fronts is 0.0045, while the percentage of warm fronts outside of the specified quadrants is 0.0013 (both averaged across ET duration). The values are normalized according to the total number of points in which the means are taken to obtain an average spatial frequency of each type of front. The trendlines in Figure 6 indicate, overall, that the average total counts of fronts are highest at ET onset for shorter ET durations, and generally get lower at ET onset as ET duration increases. The trend lines shown are statistically significant according to the Mann-Kendall test (p -value = 0.018 for warm fronts and p -value = 0.002 for cold fronts). For ET durations less than 36 hours, there is a slight increase in the frequency of both cold and warm fronts with increasing ET duration. The relationship indicated between ET duration and the number of fronts at ET onset is most prominent for ET durations longer than 36 hours, though at shorter ET durations, the values are generally more noisy. Due to the lower frequencies of longer ET durations (shown in the left panel of Figure 6), small sample sizes may play a role in the noise of the values at longer ET durations. This analysis indicates a possible connection between how long a TC takes to undergo ET and the spatial coverage and distribution of cold or warm fronts present at ET onset.

To further analyze the length of ET duration and spatial distribution of fronts, we next consider global storm-centered composites of 900 hPa frontal frequencies at the time of ET onset and the time of ET completion for the subsets of events with short ET duration (less than 36 hours) and long ET duration (longer than 36 hours) for warm fronts (Figure 7) and cold fronts (Figure 8). At the time of ET onset, there is a higher frequency of warm and cold fronts for the events that have a short ET duration, compared to those with a long ET duration. There are larger magnitude differences between short and long ET duration in the spatial distribution of cold fronts at ET onset (bottom left panel in Figure 8) compared to warm fronts at ET onset (bottom left panel of Figure 8). There is more of a zonal component to the warm frontal structure at ET completion for the long ET duration (blue colors in lower right panel of Figure 7), while there are more cold fronts present generally at ET completion for longer ET durations (blue colors in lower right panel of Figure 8).

TCs that undergo ET in less than 36 hours may thus have a contribution from pre-existing fronts contributing to a quicker transition within the CPS to an asymmetric storm, with a narrower distribution of warm frontal frequencies around 45° for the warm fronts (see top right panel of Figure 7). These results suggest that a greater occurrence of pre-existing fronts prior to the start of ET may contribute to a shorter ET duration, with the presence of more fronts implying greater baroclinicity and shear in the region. Since ET duration could be sensitive to how long TCs are tracked, we test the sensitivity of our results to the method of tracking by generating Figures 6, 7, and 8 based on IBTrACS (as in Jones et al. 2021), as well as based on IBTrACS plus extensions into the extratropical phase generated using ExTraTrack (Zarzycki et al., 2017) from Bower et al. (2022). While the exact quantitative values in these figures are different from our main results, we find that the PDF of ET duration, the average spatial frequencies of cold and warm fronts, and the spatial distributions of cold and warm fronts partitioned by short versus long ET are qualitatively similar (not shown).

3.5 | WBCs and Warm Frontal Orientations

Composites of the frequencies of warm fronts at 900hPa split between the NATL and WPAC indicate differences in the spatial distribution between each of these basins (Figure 9). In the NATL, the preferential orientation of warm fronts is northeastward from the center, while in the WPAC, there is a component of the warm frontal frequencies exhibiting an eastward protrusion, becoming more zonal with distance from the TC center. Within 500 km of the TC center extending out to 1000 km for this analysis with WBCs), the average bearing of the maximum warm frontal frequency in the NATL is 23.6° , while for the WPAC it is 37.4° (based on X markers in top panels of Figure 9). At distances greater than 500 km, the average bearing of the maximum warm frontal frequency in the NATL is 38.3° , while for the WPAC it is 64.6° (based on X markers in locations outside of 500 km in top panels of Figure 9). It is curious to note that these orientations are somewhat similar to the climatological orientations of the WBCs in each respective basin: the GS in the NATL and the Kuroshio in the WPAC. In the unseparated GS region, the average bearing between successive maxima in the ∇ SST is 55.4° , while the average bearing between successive maxima in the separated GS region is 77.6° (based on X markers closest to the coast and further away in bottom left panel of Figure 9). In the region of the Kuroshio closest to Japan, the average bearing between successive maxima in the ∇ SST is 80.1° , while further out in the Pacific the average bearing between successive maxima is 76.6° (based on X markers closest to the coast and further away in bottom right panel of Figure 9). The GS is more northeasterly-oriented for longer compared to the Kuroshio extension, with a similar orientation of the average bearings of the maximum warm frontal frequencies at ET completion in the NATL and WPAC, respectively.

A similar relationship was also found in recent work undertaken by Tochimoto and Niino (2022), who used a frontal diagnostic from Hewson (1998) to analyze the spatial structure of developing fronts in midlatitude winter cyclones relative to their time of maximum deepening rate in three different basins: the NATL, the WPAC and the Okhotsk Sea. They found that the orientations of warm frontal position in cyclone-centered composites in the WPAC and NATL matched the climatological orientations of the GS and Kuroshio extensions (and the different associated SST distributions) in those basins as well. The authors speculate that low-level frontogenesis along the SST fronts is responsible for the differences. This could be the result of the thermal dampening and strengthening mechanism (Parfitt et al., 2016), where if the temperature gradients of the SST front are sufficiently large enough and the overlying atmospheric front has the same sign of temperature gradients, then differential sensible heating across the SST front will act to strengthen the atmospheric front as it crosses the SST front. This thermal damping and strengthening mechanism has been considered in other studies (Parfitt and Kwon, 2020). We speculate that this *could* be a mechanism by which the orientation of the climatological ∇ SST "imprints" on the structure of warm frontal boundaries in the composite of

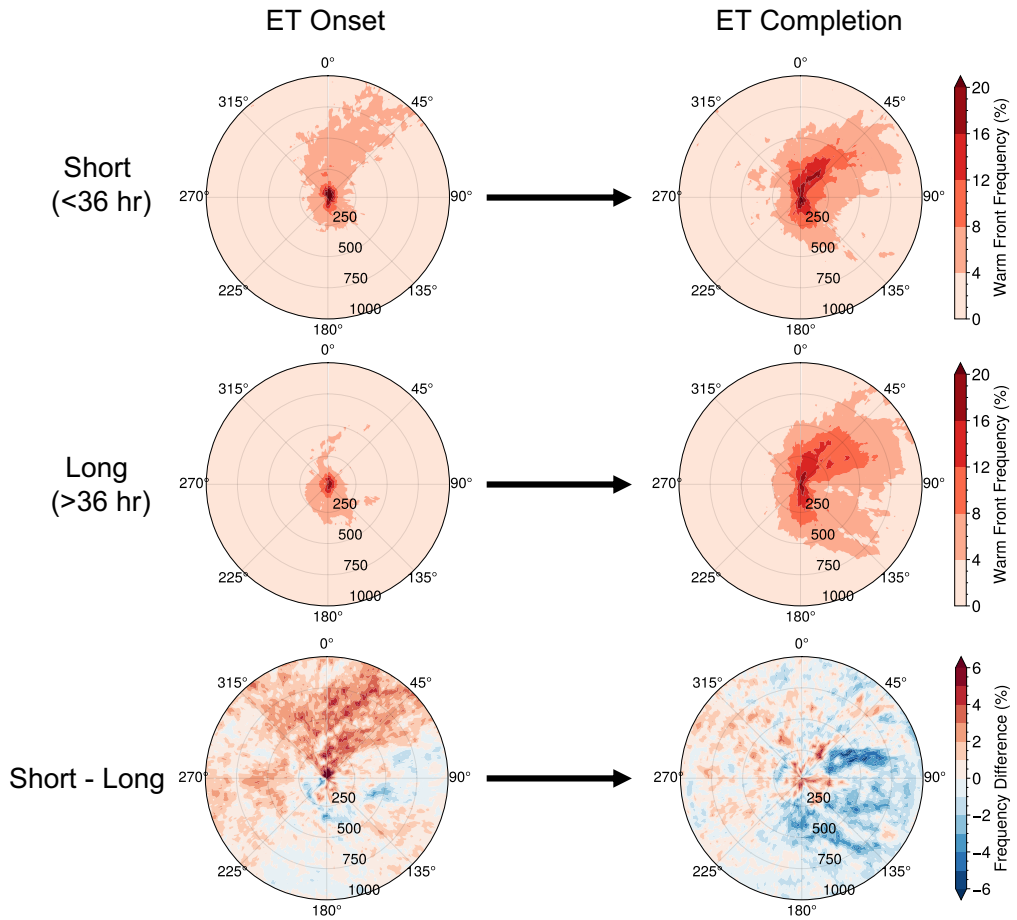


FIGURE 7 Storm-centered composites of the frequencies of 900hPa F diagnostic warm fronts for global TCs at ET onset (left) and ET completion (right) composited for ET durations less than 36 hours (top) and ET durations greater than 36 hours (middle). Warm frontal frequency composite difference (top minus middle panels) between short and long ET durations (bottom). 0° is oriented poleward.

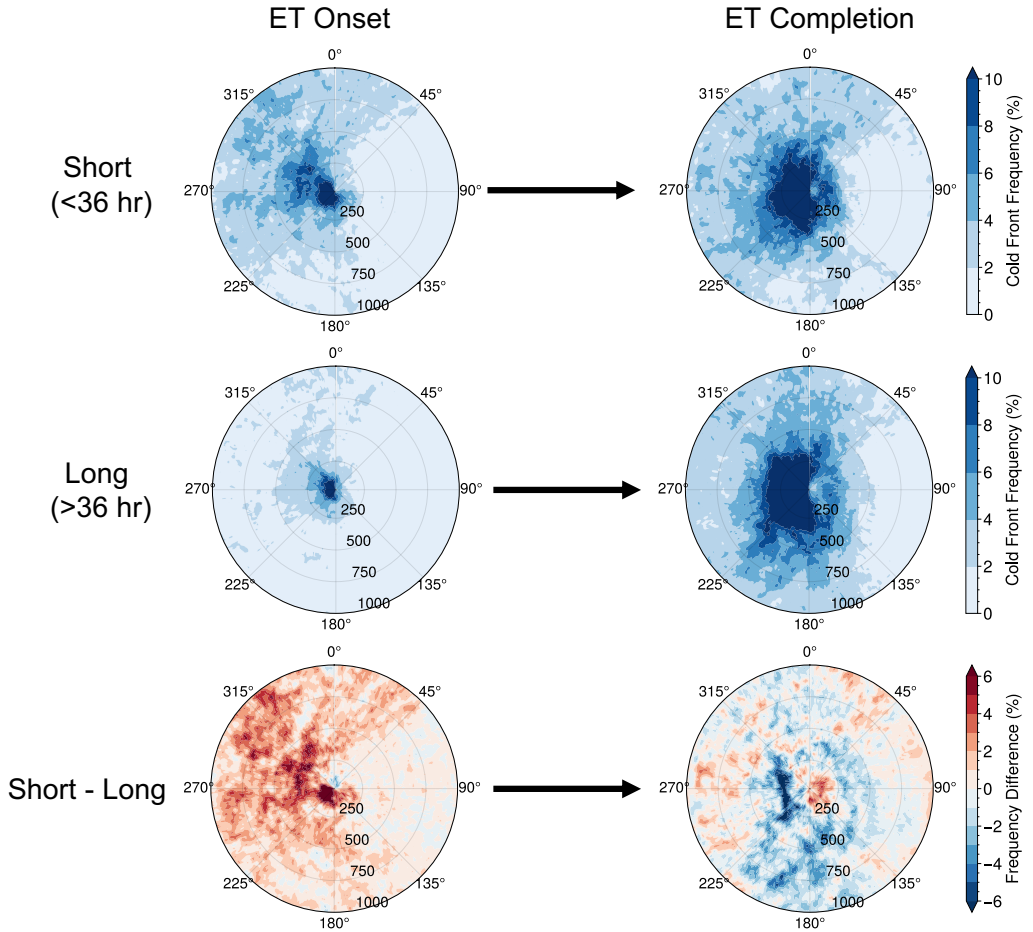


FIGURE 8 Storm-centered composites of the frequencies of 900hPa F diagnostic cold fronts for global TCs at ET onset (left) and ET completion (right) composited for ET durations less than 36 hours (top) an ET durations greater than 36 hours (bottom). Cold frontal frequency composite difference (top minus middle panels) between short and long ET durations (bottom). 0° is oriented poleward.

Figure 9.

If the above process is occurring, given the average region in which warm fronts develop during ET (as shown in Figure 4), the warm fronts that develop in TCs undergoing ET in each of these basins could align with the direction of the climatological SSTs associated with the WBCs in the respective basins. Even though each TC may or may not pass directly over a WBC, a preconditioning of the lower atmosphere combined with remote impacts from this preconditioning could exert an influence on how the warm fronts are ultimately aligned in a composite sense. For instance, a marked increase in the strength of the ∇ SST associated with either the GS or Kuroshio would result in anomalous heat exchange at the surface, possible anomalous frontogenesis (as previous work has suggested, such as Reeder et al. 2021), and even anomalous moisture vapor transport into the TC as a remote impact (as Fujiwara et al. 2020 show).

4 | CONCLUSION

This work presents the first, to our knowledge, global characterization of frontal development during ET, using both frontogenesis and an objective frontal identification metric, the F diagnostic. We first analyze composites of global TCs undergoing ET within the CPS and compare this to 500 km average 900hPa frontogenesis and SSTs. The analysis shows that fronts preferentially form at lower-levels for transitioning storms that first become asymmetric while maintaining their warm-core, while colder SSTs are first encountered for storms that lose their warm core prior to becoming asymmetric. An analysis of area-averaged adiabatic frontogenesis composited relative to ET onset and ET completion demonstrates that most of the changes in frontogenesis appear in the lower atmosphere. Thus, all subsequent analysis focuses on the lower atmosphere. Storm-centered composites of cold fronts and warm fronts identified using the F diagnostic at 900hPa shows that warm fronts preferentially form in more confined spatial regions compared to cold fronts, but generally follow the conceptual models for extratropical cyclones.

The orientation of cold and warm fronts at ET completion across poleward-, storm motion-, and shear-relative composites is consistent given the typical environmental flow during ET. An analysis of frontal development relative to ET duration shows that as ET duration increases, there are decreasing values of the average frequencies of both frontal types at ET onset. There are also more warm and cold fronts at ET onset when ET duration is less than 36 hours compared to longer ET durations, suggesting that pre-existing fronts may help ET complete more quickly. Finally, the orientations of warm fronts at ET completion in the NATL and WPAC appear to match the climatological spatial orientation of the GS and Kuroshio WBCs in those respective basins. It is unclear from this analysis exactly how large-scale spatial or temporal controls dominate the frontal development during ET, but the results provide an overview of the frontal development during ET, indicate a relationship to the duration of ET and differences across basins, and show that, in general, the fronts develop during ET as expected from prior work. The results also provide support for the growing body of evidence indicating the importance of surface conditions in frontal formation, both during ET and for frontal formation in general.

Our contextualization of where fronts form during ET has implications for where the greatest hazards will occur. For example, as fronts are where the precipitation can be quite heavy, establishing a climatology of where they form and what may influence their development informs the expected spatial distribution of rainfall. Along these fronts, gusty winds can occur as well, consistent with a broadening of the storm's wind field. In addition, the broadening wind field means a greater danger from storm surge for coastal communities. Knowledge of frontal variability in a region prior to the arrival of a TC undergoing ET can potentially provide information about how that ET proceeds. In the context of prior studies that have shown that frontal variability can be driven by ocean variability (which has a much

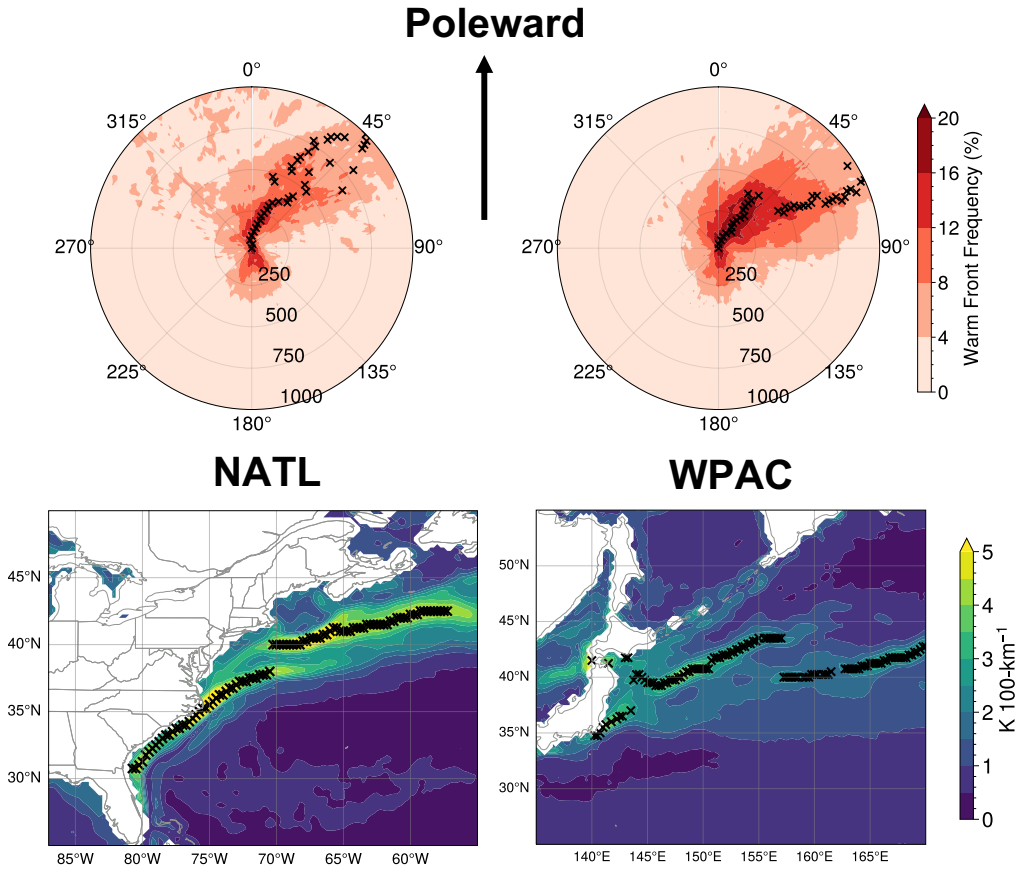


FIGURE 9 Top: TC-centered composites of 900hPa F diagnostic frequencies of warm fronts at ET completion for NATL (left) and WPAC (right) X markers indicate the maximum warm frontal frequencies at 25 km radius bins. Bottom: Climatological mean ERA5 ∇ SST (1979-2020 annual mean) for the GS and Kuroshio. X markers indicate the maximum ∇ SST at each longitude.

longer lead time) in WBC regions, this can have implications for predictability.

There are some important limitations to note for these results. Use of TC tracks from TempestExtremes, while representative of storms that actually occurred in ERA5, may introduce some uncertainty since cyclones are not necessarily tracked deep into their extratropical phase. The TCs that are transitioning are not further delineated based on type of ET (warm seclusion, etc.; see Hart et al. 2006 and Sarro and Evans 2022), which could provide further insight into contributing mechanisms. As this is work based on a reanalysis, it is subject to known biases in reanalysis representation of TCs (Hart and Evans, 2001; Schenkel and Hart, 2012; Hodges et al., 2017; Jones et al., 2021; Zarzycki et al., 2021; Slocum et al., 2022) and limitations in their ability to simulate smaller-scale processes important to frontal air-sea interaction. Our application of a 500-km length criteria for frontal identification could lead to the exclusion of important frontal variability at shorter spatial scales; however, these would be included in our analysis of the frontogenesis. Future research could include delineating the developing frontal structures between different post-ET structures (such as warm seclusion) and paths through the CPS. Additional investigation into how the frontal diagnostic used and the parameters selected affects the representation of frontal development during ET is also an area for future work. To further consider causal mechanisms behind possible surface forcing in the development of frontal structures during ET, ongoing work investigates the response of ET to perturbations in the SST pattern in a case study model simulation. Preliminary results from that work suggest that the SST pattern does influence ET and the development of fronts in the vicinity of WBCs.

Acknowledgements

The TempestExtremes TC tracks were provided by Dr. Colin Zarzycki of The Pennsylvania State University and the ExTraTrack-based extensions to TC tracks used in a sensitivity test were provided by Erica Bower and Dr. Kevin Reed of Stony Brook University. We thank Dr. Zarzycki and Dr. Reed for useful discussions about the TempestExtremes and ExTraTrack tracks. We thank Fred Soster for the downloading of ERA5 data and calculations of the F Diagnostic. We thank Dr. Robert Hart for his insights into the cyclone phase space and feedback on the content of this study. RP gratefully acknowledges support from NSF OCE 2023585, and support from NOAA's Climate Program Office, Climate Variability and Predictability Program NA22OAR4310617.

Conflict of Interest

The authors declare no conflict of interest.

Data Availability Statement

The data that support the findings of this study are available from the corresponding author upon reasonable request.

references

- Aarons, Z. S., Camargo, S. J., Strong, J. D. and Murakami, H. (2021) Tropical Cyclone Characteristics in the MERRA-2 Reanalysis and AMIP Simulations. *Earth and Space Science*, **8**.
- Bieli, M., Camargo, S. J., Sobel, A. H., Evans, J. L. and Hall, T. (2019a) A global climatology of extratropical transition. Part I: Characteristics across basins. *Journal of Climate*, **32**, 3557–3582.

- (2019b) A global climatology of extratropical transition. Part II: Statistical performance of the cyclone phase space. *Journal of Climate*, **32**, 3583–3597.
- Bluestein, H. (1993) *Observations and Theory of Weather Systems. Vol. 2, Synoptic-Dynamic Meteorology in Midlatitudes*. Oxford University Press.
- Booth, J. F., Thompson, L., Patoux, J. and Kelly, K. A. (2012) Sensitivity of midlatitude storm intensification to perturbations in the sea surface temperature near the Gulf Stream. *Monthly Weather Review*, **140**, 1241–1256.
- Bower, E., Reed, K. A., Ullrich, P. A., Zarzycki, C. M. and Pendergrass, A. G. (2022) Quantifying Heavy Precipitation throughout the Entire Tropical Cyclone Life Cycle. *Journal of Hydrometeorology*, **23**, 1645–1662.
- Bright, R. J., Xie, L. and Pietrafesa, L. J. (2002) Evidence of the Gulf Stream's influence on tropical cyclone intensity. *Geophysical Research Letters*, **29**, 48–1–48–4.
- Businger, S., Graziano, T. M., Kaplan, M. L. and Rozumalski, R. A. (2005) Cold-air cyclogenesis along the Gulf-Stream front: Investigation of diabatic impacts on cyclone development, frontal structure, and track. *Meteorology and Atmospheric Physics*, **88**, 65–90.
- Cione, J. J., Raman, S. and Pietrafesa, L. J. (1993) The effect of Gulf Stream-induced baroclinicity on U.S. East Coast winter cyclones. *Monthly Weather Review*, **121**, 421–430.
- Compo, G. P., Whitaker, J. S., Sardeshmukh, P. D., Matsui, N., Allan, R. J., Yin, X., Gleason, B. E., Vose, R. S., Rutledge, G., Bessemoulin, P., BroNnimann, S., Brunet, M., Crouthamel, R. I., Grant, A. N., Groisman, P. Y., Jones, P. D., Kruk, M. C., Kruger, A. C., Marshall, G. J., Maugeri, M., Mok, H. Y., Nordli, O., Ross, T. F., Trigo, R. M., Wang, X. L., Woodruff, S. D. and Worley, S. J. (2011) The Twentieth Century Reanalysis Project. *Quarterly Journal of the Royal Meteorological Society*, **137**, 1–28.
- Duvel, J. P., Camargo, S. J. and Sobel, A. H. (2017) Role of the convection scheme in modeling initiation and intensification of tropical depressions over the North Atlantic. *Monthly Weather Review*, **145**, 1495–1509.
- Emanuel, K. (2018) 100 Years of Progress in Tropical Cyclone Research. *Meteorological Monographs*, **59**, 15.1–15.68.
- Evans, C., Wood, K. M., Aberson, S. D., Archambault, H. M., Milrad, S. M., Bosart, L. F., Corbosiero, K. L., Davis, C. A., Pinto, J. R., Doyle, J., Fogarty, C., Galarneau, T. J., Grams, C. M., Griffin, K. S., Gyakum, J., Hart, R. E., Kitabatake, N., Lentink, H. S., Mctaggart-Cowan, R., Perrie, W., Quinting, J. F., Reynolds, C. A., Riemer, M., Ritchie, E. A., Sun, Y. and Zhang, F. (2017) The extratropical transition of tropical cyclones. Part I: Cyclone evolution and direct impacts. *Monthly Weather Review*, **145**, 4317–4344.
- Evans, J. L. and Hart, R. E. (2003) Objective indicators of the life cycle evolution of extratropical transition for Atlantic tropical cyclones. *Monthly Weather Review*, **131**, 909–925.
- Fujiwara, K., Kawamura, R. and Kawano, T. (2020) Remote Thermodynamic Impact of the Kuroshio Current on a Developing Tropical Cyclone Over the Western North Pacific in Boreal Fall. *Journal of Geophysical Research: Atmospheres*, **125**, e2019JD031356.
- Galarneau, T. J., Davis, C. A. and Shapiro, M. A. (2013) Intensification of hurricane sandy (2012) through extratropical warm core seclusion. *Monthly Weather Review*, **141**, 4296–4321.
- Hart, R. E. (2003) A cyclone phase space derived from thermal wind and thermal asymmetry. *Monthly Weather Review*, **131**, 585–616.
- Hart, R. E. and Evans, J. L. (2001) A climatology of the extratropical transition of Atlantic tropical cyclones. *Journal of Climate*, **14**, 546–564.
- Hart, R. E., Evans, J. L. and Evans, C. (2006) Synoptic composites of the extratropical transition life cycle of North Atlantic tropical cyclones: Factors determining posttransition evolution. *Monthly Weather Review*, **134**, 553–578.

- Hersbach, H., Bell, B., Berrisford, P., Hirahara, S., Horányi, A., Muñoz-Sabater, J., Nicolas, J., Peubey, C., Radu, R., Schepers, D., Simmons, A., Soci, C., Abdalla, S., Abellan, X., Balsamo, G., Bechtold, P., Biavati, G., Bidlot, J., Bonavita, M., De Chiara, G., Dahlgren, P., Dee, D., Diamantakis, M., Dragani, R., Flemming, J., Forbes, R., Fuentes, M., Geer, A., Haimberger, L., Healy, S., Hogan, R. J., Hólm, E., Janisková, M., Keeley, S., Laloyaux, P., Lopez, P., Lupu, C., Radnoti, G., De Rosnay, P., Rozum, I., Vamborg, F., Villaume, S. and Thépaut, J.-N. (2020) The ERA5 global reanalysis. *Q J R Meteorol Soc*, **146**, 1999–2049.
- Hewson, T. D. (1998) Objective fronts. *Meteorological Applications*, **5**, 37–65.
- Hodges, K., Cobb, A. and Vidale, P. L. (2017) How well are tropical cyclones represented in reanalysis datasets? *Journal of Climate*, **30**, 5243–5264.
- Hsieh, J. S. and Cook, K. H. (2008) On the instability of the African easterly jet and the generation of African waves: Reversals of the potential vorticity gradient. *Journal of the Atmospheric Sciences*, **65**, 2130–2151.
- Jacobs, N. A., Raman, S., Lackmann, G. M. and Childs, P. P. (2008) The influence of the Gulf Stream induced SST gradients on the US East Coast winter storm of 24–25 January 2000. *International Journal of Remote Sensing*, **29**, 6145–6174.
- Jenkner, J., Sprenger, M., Schwenk, I., Schwierz, C., Dierer, S. and Leuenberger, D. (2010) Detection and climatology of fronts in a high-resolution model reanalysis over the Alps. *Meteorological Applications*, **17**, 1–18.
- Jones, E., Parfitt, R., Wing, A. A. and Hart, R. (2023) Gulf Stream Sea Surface Temperature Anomalies Associated With the Extratropical Transition of North Atlantic Tropical Cyclones. *Geophysical Research Letters*, **50**, 1–10.
- Jones, E., Wing, A. A. and Parfitt, R. (2021) A global perspective of tropical cyclone precipitation in reanalyses. *Journal of Climate*, **34**, 8461–8480.
- Jones, S. C., Harr, P. A., Abraham, J., Bosart, L. F., Bowyer, P. J., Evans, J. L., Hanley, D. E., Hanstrum, B. N., Hart, R. E., Lalaurette, F., Sinclair, M. R., Smith, R. K. and Thorncroft, C. (2003) The extratropical transition of tropical cyclones: Forecast challenges, current understanding, and future directions. *Weather and Forecasting*, **18**, 1052–1092.
- Jung, C. and Lackmann, G. M. (2021) The response of extratropical transition of tropical cyclones to climate change: Quasi-idealized numerical experiments. *Journal of Climate*, **34**, 4361–4381.
- Keller, J. H., Grams, C. M., Riemer, M., Archambault, H. M., Bosart, L., Doyle, J. D., Evans, J. L., Galarneau, T. J., Griffin, K., Harr, P. A., Kitabatake, N., McTaggart-Cowan, R., Pantillon, F., Quinting, J. F., Reynolds, C. A., Ritchie, E. A., Torn, R. D. and Zhang, F. (2019) The extratropical transition of tropical cyclones. Part II: Interaction with the midlatitude flow, downstream impacts, and implications for predictability. *Monthly Weather Review*, **147**, 1077–1106.
- Kim, D., Sobel, A. H., Genio, A. D., Chen, Y., Camargo, S. J., Yao, M. S., Kelley, M. and Nazarenko, L. (2012) The tropical subseasonal variability simulated in the nasa giss general circulation model. *Journal of Climate*, **25**, 4641–4659.
- Kitabatake, N. (2008) Extratropical Transition of Tropical Cyclones in the Western North Pacific: Their Frontal Evolution. *Monthly Weather Review*, **136**, 2066–2090.
- Klein, P. M., Harr, P. A. and Elsberry, R. L. (2000) Extratropical Transition of Western North Pacific Tropical Cyclones: An Overview and Conceptual Model of the Transformation Stage. *Weather and Forecasting*, **15**, 373–395.
- Knapp, K. R., Kruk, M. C., Levinson, D. H., Diamond, H. J. and Neumann, C. J. (2010) The international best track archive for climate stewardship (IBTrACS). *Bulletin of the American Meteorological Society*, **91**, 363–376.
- Kobayashi, S., Ota, Y., Harada, Y., Ebata, A., Moriya, M., Onoda, H., Onogi, K., Kamahori, H., Kobayashi, C., Endo, H., Miyaoka, K. and Kiyotoshi, T. (2015) The JRA-55 reanalysis: General specifications and basic characteristics. *Journal of the Meteorological Society of Japan*, **93**, 5–48.
- Kofron, D. E., Ritchie, E. A. and Tyo, J. S. (2010) Determination of a Consistent Time for the Extratropical Transition of Tropical Cyclones. Part II: Potential Vorticity Metrics. *Monthly Weather Review*, **138**, 4344–4361.

- Lawrence, L., Parfitt, R. and Ummenhofer, C. C. (2022) The role of atmospheric fronts in austral winter precipitation changes across Australia. *Atmospheric Science Letters*, e1117.
- Li, Q. and Wang, Q. (2013) Re-examination of the potential vorticity metrics for determining extratropical transition onset and completion times using high-resolution data. *Acta Meteorologica Sinica*, **27**, 502–508.
- Mak, M., Lu, Y. and Deng, Y. (2017) Two issues concerning surface frontogenesis. *Journal of the Atmospheric Sciences*, **74**, 2967–2987.
- McCarty, W., Coy, L., Gelaro, R., Huang, A., Merkova, D., Smith, E. B., Sienkiewicz, M. and Wargan, K. (2016) (34) MERRA-2 Input Observations: Summary and Assessment. *Technical Report Series on Global Modeling and Data Assimilation*, **46**, 1–40.
- Michaelis, A. C. and Lackmann, G. M. (2019) Climatological changes in the extratropical transition of tropical cyclones in high-resolution global simulations. *Journal of Climate*, **32**, 8733–8753.
- (2021) Storm-scale dynamical changes of extratropical transition events in present-day and future high-resolution global simulations. *Journal of Climate*, **34**, 5037–5062.
- Murakami, H., Wang, Y., Yoshimura, H., Mizuta, R., Sugi, M., Shindo, E., Adachi, Y., Yukimoto, S., Hosaka, M., Kusunoki, S., Ose, T. and Kitoh, A. (2012) Future changes in tropical cyclone activity projected by the new high-resolution MRI-AGCM. *Journal of Climate*, **25**, 3237–3260.
- Parfitt, R., Czaja, A. and Kwon, Y.-O. (2017) The impact of SST resolution change in the ERA-Interim reanalysis on wintertime Gulf Stream frontal air-sea interaction. *Geophysical Research Letters*, **44**, 3246–3254.
- Parfitt, R., Czaja, A., Minobe, S. and Kuwano-Yoshida, A. (2016) The atmospheric frontal response to SST perturbations in the Gulf Stream region. *Geophysical Research Letters*, **43**, 2299–2306.
- Parfitt, R. and Kwon, Y. O. (2020) The modulation of gulf stream influence on the troposphere by the eddy-driven jet. *Journal of Climate*, **33**, 4109–4120.
- Petterssen, S. (1936) *Contribution to the theory of frontogenesis*. Geofysiske Publikasjoner.
- Powell, S. W. and Bell, M. M. (2019) Near-surface frontogenesis and atmospheric instability along the u.s. east coast during the extratropical transition of hurricane matthew (2016). *Monthly Weather Review*, **147**, 719–732.
- Reed, K. A. and Jablonowski, C. (2011) Impact of physical parameterizations on idealized tropical cyclones in the Community Atmosphere Model. *Geophysical Research Letters*, **38**, n/a–n/a.
- Reeder, M. J., Spengler, T. and Spensberger, C. (2021) The Effect of Sea Surface Temperature Fronts on Atmospheric Frontogenesis. *Journal of the Atmospheric Sciences*, **78**, 1753–1771.
- Saha, S., Moorthi, S., Pan, H. L., Wu, X., Wang, J., Nadiga, S., Tripp, P., Kistler, R., Woollen, J., Behringer, D., Liu, H., Stokes, D., Grumbine, R., Gayno, G., Wang, J., Hou, Y. T., Chuang, H. Y., Juang, H. M. H., Sela, J., Iredell, M., Treadon, R., Kleist, D., Van Delst, P., Keyser, D., Derber, J., Ek, M., Meng, J., Wei, H., Yang, R., Lord, S., Van Den Dool, H., Kumar, A., Wang, W., Long, C., Chelliah, M., Xue, Y., Huang, B., Schemm, J. K., Ebisuzaki, W., Lin, R., Xie, P., Chen, M., Zhou, S., Higgins, W., Zou, C. Z., Liu, Q., Chen, Y., Han, Y., Cucurull, L., Reynolds, R. W., Rutledge, G. and Goldberg, M. (2010) The NCEP climate forecast system reanalysis. *Bulletin of the American Meteorological Society*, **91**, 1015–1057.
- Sarro, G. and Evans, C. (2022) An Updated Investigation of Post-Transformation Intensity, Structural, and Duration Extremes for Extratropically Transitioning North Atlantic Tropical Cyclones. *Monthly Weather Review*, **150**, 2911–2933.
- Schemm, S., Rudeva, I. and Simmonds, I. (2015) Extratropical fronts in the lower troposphere-global perspectives obtained from two automated methods. *Quarterly Journal of the Royal Meteorological Society*, **141**, 1686–1698.
- Schemm, S. and Sprenger, M. (2015) Frontal-wave cyclogenesis in the North Atlantic -a climatological characterisation. *Quarterly Journal of the Royal Meteorological Society*, **141**, 2989–3005.

- Schemm, S., Sprenger, M. and Wernli, H. (2018) When during Their Life Cycle Are Extratropical Cyclones Attended by Fronts? *Bulletin of the American Meteorological Society*, **99**, 149–165.
- Schenkel, B. A. and Hart, R. E. (2012) An examination of tropical cyclone position, intensity, and intensity life cycle within atmospheric reanalysis datasets. *Journal of Climate*, **25**, 3453–3475.
- Seethala, C., Zuidema, P., Edson, J., Brunke, M., Chen, G., Li, X. Y., Painemal, D., Robinson, C., Shingler, T., Shook, M., Sorooshian, A., Thornhill, L., Tornow, F., Wang, H., Zeng, X. and Ziemba, L. (2021) On Assessing ERA5 and MERRA2 Representations of Cold-Air Outbreaks Across the Gulf Stream. *Geophysical Research Letters*, **48**.
- Seikioka, M. (1957) A Hypothesis on Complex of Tropical and Extratropical Cyclones for Typhoon in the Middle Latitudes. III. Examples of Typhoon not accompanied by Extratropical Cyclone in the Middle Latitudes. *Journal of the Meteorological Society of Japan. Ser. II*, **35**, 170–173.
- Slocum, C. J., Razin, M. N., Knaff, J. A. and Stow, J. P. (2022) Does ERA5 Mark a New Era for Resolving the Tropical Cyclone Environment? *Journal of Climate*, **35**, 3547–3564.
- Soster, F. and Parfitt, R. (2022) On Objective Identification of Atmospheric Fronts and Frontal Precipitation in Reanalysis Datasets. *Journal of Climate*, **35**, 4513–4534.
- Spensberger, C. and Sprenger, M. (2018) Beyond cold and warm: an objective classification for maritime midlatitude fronts. *Quarterly Journal of the Royal Meteorological Society*, **144**, 261–277.
- Thomas, C. M. and Schultz, D. M. (2019) Global climatologies of fronts, airmass boundaries, and airstream boundaries: Why the definition of “front” matters. *Monthly Weather Review*, **147**, 691–717.
- Tochimoto, E. and Niino, H. (2022) Comparing Frontal Structures of Extratropical Cyclones in the Northwestern Pacific and Northwestern Atlantic Storm Tracks. *Monthly Weather Review*, **150**, 369–392.
- Tsopouridis, L., Spengler, T. and Spensberger, C. (2021) Smoother versus sharper Gulf Stream and Kuroshio sea surface temperature fronts: effects on cyclones and climatology. *Weather and Climate Dynamics*, **2**, 953–970.
- Tsopouridis, L., Spensberger, C. and Spengler, T. (2020) Characteristics of cyclones following different pathways in the Gulf Stream region. *Quarterly Journal of the Royal Meteorological Society*, **147**, 392–407.
- Ullrich, P. A. and Zarzycki, C. M. (2017) TempestExtremes: A framework for scale-insensitive pointwise feature tracking on unstructured grids. *Geoscientific Model Development*, **10**, 1069–1090.
- Velden, C. S. and Sears, J. (2014) Computing deep-tropospheric vertical wind shear analyses for tropical cyclone applications: Does the methodology matter? *Weather and Forecasting*, **29**, 1169–1180.
- Zarzycki, C. M., Thatcher, D. R. and Jablonowski, C. (2017) Objective tropical cyclone extratropical transition detection in high-resolution reanalysis and climate model data. *Journal of Advances in Modeling Earth Systems*, **9**, 130–148.
- Zarzycki, C. M. and Ullrich, P. A. (2017) Assessing sensitivities in algorithmic detection of tropical cyclones in climate data. *Geophysical Research Letters*, **44**, 1141–1149.
- Zarzycki, C. M., Ullrich, P. A. and Reed, K. A. (2021) Metrics for evaluating tropical cyclones in climate data. *Journal of Applied Meteorology and Climatology*, **60**, 643–660.
- Zhao, M., Held, I. M. and Lin, S. J. (2012) Some counterintuitive dependencies of tropical cyclone frequency on parameters in a GCM. *Journal of the Atmospheric Sciences*, **69**, 2272–2283.
- Zhou, Y., Xiao, K. and Song, H. (2012) Diagnosis of the developmental mechanism of the extratropical transition of a tropical cyclone using potential vorticity inversion of frontogenesis. *Journal of Tropical Meteorology*, **18**, 360–368.